GPS Solutions (2024) 28:121
https://doi.org/10.1007/s10291-024-01663-1

ORIGINAL ARTICLE

# Can the phase of SNR oscillations in GNSS-IR be used to estimate sea-level height?

**Zhenkui Wei[1] · Chao Ren[1] · Yueji Liang[1] · Yintao Liu[1] · Jieyu Liang[1] · Anchao Yin[1] · Weiting Yue[1] · Xudong Zhang[1] · Xiaoqi Lin[1]**

Received: 27 September 2023 / Accepted: 23 April 2024


**Abstract**
In existing global navigation satellite system-interference reflectometry (GNSS-IR) research, only the frequency of signal-to-noise ratio (SNR) oscillations has been used to estimate sea-level height. However, the characteristic parameters of SNR oscillations are not isolated from each other, and a single feature cannot accurately and comprehensively capture the environmental changes of reflecting surface. Our simulation results show that for the nonlinear least squares (NLS), when there is a certain difference between the fitting frequency and the actual frequency of SNR oscillations, the deviation of the phase solution obtained is approximately linear with the frequency difference. Consequently, a linear phase correction GNSS-IR sea-level estimation method is constructed in this study. This method integrates the Lomb–Scargle periodogram (LSP) and NLS to process SNR oscillations, using the phase obtained from NLS to correct the retrieval error of LSP. Through processing SNR data from four sites for nearly half a year, we verified the stability of the relationship between phase and frequency-based retrieval error at different sites in continuous monitoring, and established the relationship model between the two. Then, utilizing the relationship model acquired at different sites, we estimated the sea-level variations for the next 6 months at each site through joint frequency and phase versus reflector height relationships. Experimental results show that the phases acquired from NLS can effectively correct the retrieval error of LSP. Compared with the traditional method using only frequency, the root mean square error and mean absolute error of the retrieval results obtained from the linear phase correction GNSS-IR sea-level estimation method based on LSP-NLS are both reduced by about 60%. This multi-feature fusion technique introduces a new perspective and technical approach for GNSS-IR sea-level estimations.

**Keywords** GNSS-IR · Sea-level estimation · SNR oscillations · NLS · Linear phase correction

## Introduction

In 2008, Larson et al. (2008) proposed a global navigation satellite system-interference reflectometry (GNSS-IR) technique based on signal-to-noise ratio (SNR) oscillations. This technique utilizes SNR data from a standard geodetic receiver to obtain the physical parameters of the reflecting surface. It has been widely applied in various fields, such as snow depth (Larson et al. 2009; Larson and Nievinski 2013), soil moisture (Chew et al. 2013; Ran et al. 2022), storm surges (Peng et al. 2019; Larson et al. 2021), and vegetation changes (Li et al. 2023; Zhang et al. 2021).

In 2013, Larson et al. (2013a) systematically described a general method for retrieving sea-level heights using GNSS-IR techniques. To further enhance the precision of this technique, existing research has primarily focused on four areas: (1) dynamic correction of sea level (Larson et al. 2013b, 2017); (2) tropospheric delay (Santamaría-Gómez and Watson 2017; Williams and Nievinski 2017); (3) direct and reflected signal separation (Wang et al. 2018b; Hu et al. 2021); (4) multi-mode and multi-frequency data fusion (Roussel et al. 2015; Wang et al. 2019a). Furthermore, Wang et al. (2018a) analyzed the SNR data from the PBAY, SC02, and BRST sites, determining the optimal azimuth range for each site to retrieve sea-level height. Song et al. (2019) discussed the quality control conditions in the GNSS-IR retrieval process and proposed a quality control method combining multiple parameters and external constraints, which can effectively eliminate gross errors. Strandberg

✉ Chao Ren
renchao@glut.edu.cn

[1] College of Geomatics and Geoinformation, Guilin University of Technology, Guilin 541004, China

Published online: 06 May 2024

et al. (2016, 2019) successfully retrieved real-time tide levels by combining reverse modeling technology and Kalman filtering. Meanwhile, Wang et al. (2019b) employed wavelet analysis to extract the instantaneous frequency from the SNR series, significantly enhancing the temporal resolution of the retrieval results. After years of development, GNSS-IR sea-level monitoring technology has become relatively mature.

In the GNSS-IR principle, SNR oscillations are simplified as a standard cosine function, whose characteristic parameters primarily include frequency, amplitude, and initial phase. During data processing, the Lomb–Scargle periodogram (LSP) is typically used to extract the frequency of SNR oscillations before solving for the amplitude and phase of SNR oscillations utilizing nonlinear least squares (NLS) (Li et al. 2023; Martín et al. 2020). The classical GNSS-IR altimetry methods mainly depend on LSP, and the uncertainty of LSP is the direct cause of their retrieval deviation. GNSS signals face challenges from random noise, tropospheric delays, and sea surface roughness along with its dynamic variations, all leading to a decrease in SNR quality (Ilyushin et al. 2019; Purnell et al. 2020). Moreover, factors such as sampling intervals, sequence lengths, and missing data further enhance the uncertainty of LSP (VanderPlas 2018). The combination of these factors causes a certain deviation in the retrieval results of LSP. In the "LSP + NLS" mode of data processing, the retrieval error of LSP is directly transmitted to amplitude and phase through NLS. Conversely, if the relationship of error propagation between them can be modeled, the solution results of NLS can be employed to correct the retrieval error of LSP, further improving the retrieval accuracy.

Current research has focused on exploring the impact of environmental factors on the retrieval accuracy of algorithms, often neglecting error propagation between different algorithms. To this end, we delved into the frequency-phase transfer relationship for NLS in this study. The analysis results of the simulated data show that when the frequency of the fitted function is somewhat different from the actual frequency of the SNR oscillations, the deviation of phase solution obtained by NLS will have a correspondence with the frequency difference. This implies that the retrieval error of LSP can be corrected by the phase from NLS. To verify the stability of this relationship, we processed nearly half a year of SNR data from the SC02, GTGU, SPBY, and CALC sites and analyzed the relationship between the phase and retrieval error at different sites. Following this, utilizing the derived relationship models from various sites, we estimated the sea-level variations for the next 6 months at each site, further improving the accuracy of the retrieval results.

## Site and data

SNR data of the GPS L1 band from four GNSS sites were used in this study, including GTGU (Geremia-Nievinski et al. 2020) in Sweden, SPBY (Strandberg et al. 2016) in Australia, and SC02 (Larson et al. 2017) and CALC (Wang et al. 2022) in the United States (as shown in Table 1 and Fig. 1). Among them, GTGU is a site specifically established for GNSS-reflectometry research, while the other sites are primarily used for monitoring continental plate movements. The antennas of these sites are situated near the coast, making them widely used for research related to GNSS-IR sea-level estimation. The tide gauge (TG) station near them can provide measured sea-level variations.

## Methodology

In this section, we describe the basic principle of GNSS-IR technique in detail. Then based on this principle, the relationship between the frequency difference and the deviation of phase solution of NLS was explored utilizing simulation data.

### GNSS interferometric reflectometry principle

GNSS antennas situated near the coast are capable of simultaneously receiving direct signals as well as signals reflected off the sea surface. Figure 2 illustrates the geometric principle of GNSS sea surface reflection. In the figure, $h$ is the distance from the antenna phase center to the sea level, namely, reflector height (RH); $\theta$ is the angle between the direct signal and the sea level, namely, the satellite elevation angle; and $D$ is the path difference between the direct and reflected signals.

**Table 1** SNR and TG data for each site used in this study

| Site codes | Azimuth | Elevation | Antenna height (m) | Sampling interval (s) | TG data | |
|---|---|---|---|---|---|---|
| | | | | | Distance to site | Sampling interval |
| SC02 | 50°–240° | 2°–12° | 5.5 | 15 | 300 m | 6 min |
| GTGU | 70°–260° | 1°–14.5° | 4 | 30 | 1 km | 1 min |
| SPBY | 230°–360° | 2°–12° | 4 | 30 | Same position | 1 h |
| CALC | − 140° to 70° | 5°–15° | 12 | 30 | Same position | 6 min |

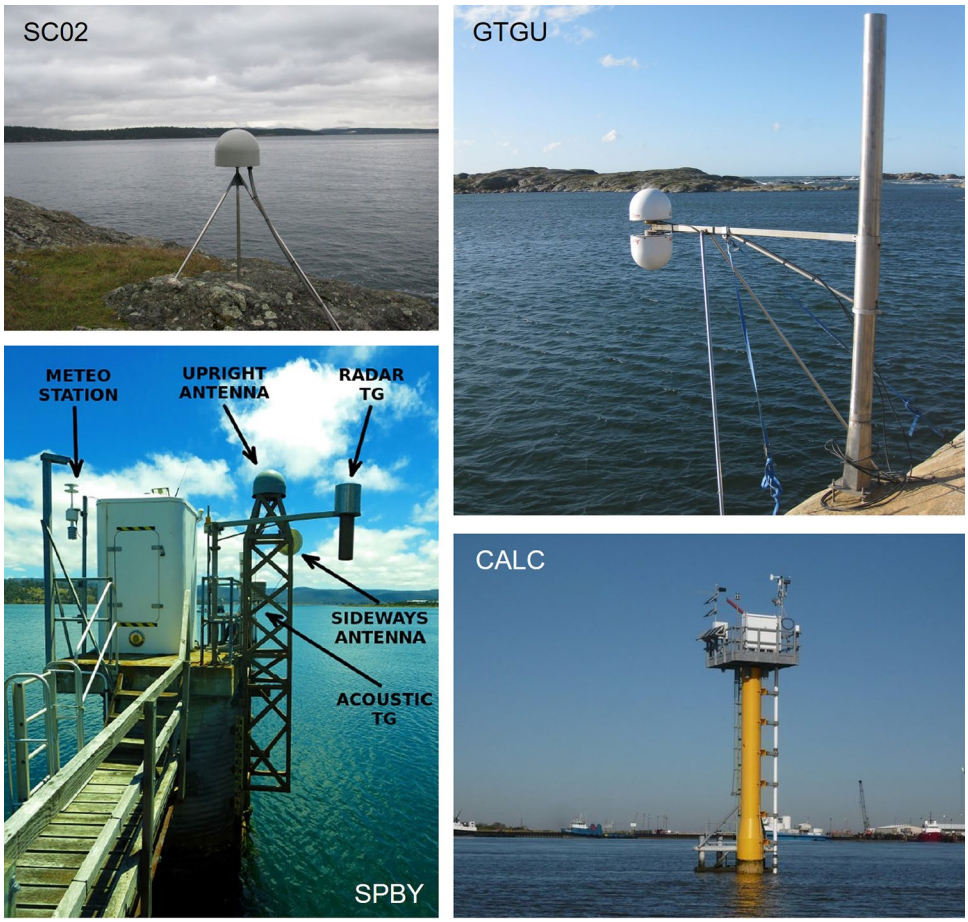


**Fig. 1** Location and environment of different sites. Sites and picture credits: SC02 (http://www.unavco.org/); GTGU (https://spotlight.unavco.org/); SPBY (https://gnss-reflections.org/); CALC (https://tidesandcurrents.noaa.gov/)

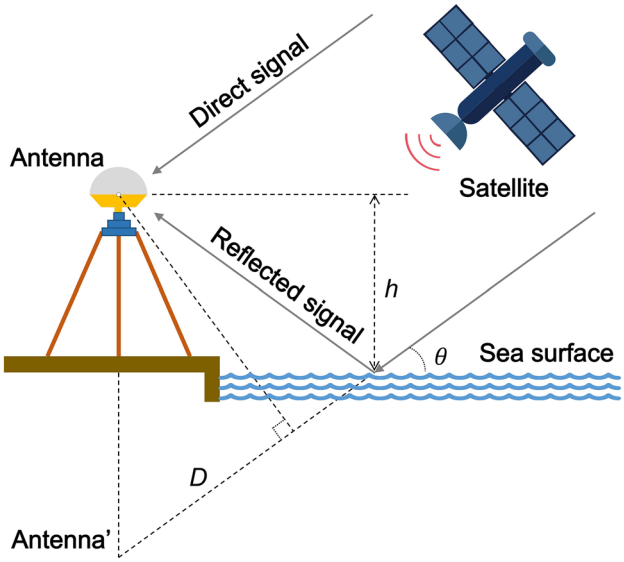


**Fig. 2** Geometric model of the GNSS sea surface reflection

From Fig. 2, it can be observed that after the reflected signal bounces off the sea surface, its path to the receiver is longer than that of the direct signal. Considering only one reflection, the path difference $D$ can be expressed as:

$$D = 2h \sin\theta \tag{1}$$

The composite signal formed by the superposition of the direct and reflected signal is recorded by the receiver in the form of SNR, which can be represented as (Roussel et al. 2015):

$$\mathrm{SNR}^2 = A_d^2 + A_m^2 + 2A_dA_m \cos\psi \tag{2}$$

where $A_d$ and $A_m$ are the direct and reflected signal amplitudes, respectively, and $\psi$ is the phase difference between the two signals. From the path difference $D$, the $\psi$ can be deduced as:

$$\psi = \frac{2\pi}{\lambda} D = \frac{4\pi h}{\lambda} \sin\theta \tag{3}$$

where $\lambda$ is the carrier wavelength. Generally, the trend term of an SNR series can be eliminated by removing a low-order polynomial from it, namely $A_d^2 + A_m^2$ (direct signal and a

small amount of reflected signal) in (2) (Bilich and Larson 2007; Löfgren et al. 2014). The remaining segment constitutes the SNR oscillation term, which can be approximated utilizing the cosine model:

$$\mathrm{SNR}_m = 2A_d A_m \cos\psi = A\cos(2\pi f x + \varphi) \tag{4}$$

where $A$ is the signal amplitude, $f$ is the frequency, and $\varphi$ is the phase. As illustrated in (3), if the dynamic variation of sea level is not considered, there is a linear relationship between the $\psi$ and $\sin\theta$, which is followed:

$$2\pi f = \frac{d\psi}{d\sin\theta} = \frac{4\pi h}{\lambda} \tag{5}$$

After simplifying (5), the relationship between the reflector height $h$ and the frequency $f$ of $\mathrm{SNR}_m$ can be derived as:

$$h = \frac{\lambda f}{2} \tag{6}$$

As shown in (6), $h$ can be calculated as long as the $f$ of SNR oscillations is obtained. However, $h$ is referenced to the antenna phase center. To determine the sea-level height, a datum conversion is also required:

$$h_{sea} = H - h \tag{7}$$

where $h_{sea}$ is the sea-level height and $H$ is the distance from the antenna phase center to the datum of TG. The SNR oscillation varies with the sine of the satellite elevation angle, forming a non-uniformly sampled series. Proposed by Lomb and further refined by Scargle, LSP is a spectrum analysis method for non-uniformly sampled series (Lomb 1976; Scargle 1982). Hence, the LSP method is generally employed in GNSS-IR techniques to extract the frequency information from SNR oscillation.

Replacing $x$ in (4) with $\sin\theta$, the relationship between SNR oscillation and $\sin\theta$ can be expressed as:

$$\mathrm{SNR}_m = A\cos(2\pi f\sin\theta + \varphi) \tag{8}$$

The oscillations of the SNR series diminish with increasing elevation angle. When it is necessary to consider this decay characteristic of the SNR oscillations, it can be further described as (Nievinski and Larson 2014):

$$\mathrm{SNR}_m = Ae^{-k\sin^2\theta}\cos(2\pi f\sin\theta + \varphi) \tag{9}$$

where $k$ is the decay factor. The $A$ and $\varphi$ of SNR oscillations are typically solved using NLS, with (8) as the objective function. The $f$ in the equation is derived from the retrieval results of the LSP (Strandberg et al. 2016; Martín et al. 2020; Marquardt 1963). SNR oscillations are only present at low-elevation ranges, typically no higher than 30°. However, due to the limitations on the horizon of the antenna and the quality of SNR data, the actual length of available SNR series may be further shortened. Within such a limited elevation range, the decay trend of SNR oscillations is not significant. This weak decay trend is susceptible to noise and may not be accurately captured when fitting SNR oscillations using NLS. In fact, if the decay factor is over-introduced, it may bring additional errors to the fitting results. Therefore, although (9) is theoretically closer to the reflection principle of GNSS signals, Eq. (8) is generally preferred as the objective function of NLS during the actual retrieval process.

## Relationship between height difference (or frequency difference) and phase difference

The fitted frequencies set in NLS are derived from the retrieval results of LSP. Due to the existence of errors, it does not match the true frequency of SNR oscillations. During the fitting process, NLS attempts to compensate for this discrepancy by adjusting the phase and amplitude (Ran et al. 2022; Vey et al. 2016; Chew et al. 2016), which leads to a deviation in phase and amplitude. Figure 3 shows the fitting results of NLS when the fitted frequency does not match the signal frequency. The signal in the figure is simulated by (9) with an amplitude of 20, a phase of 0, a frequency of 20, and a decay factor of 10. Equation (8) is used as the objective function of NLS, and the fitted frequency is set to 19.5. To generate a non-uniform sampling series, a specific range of

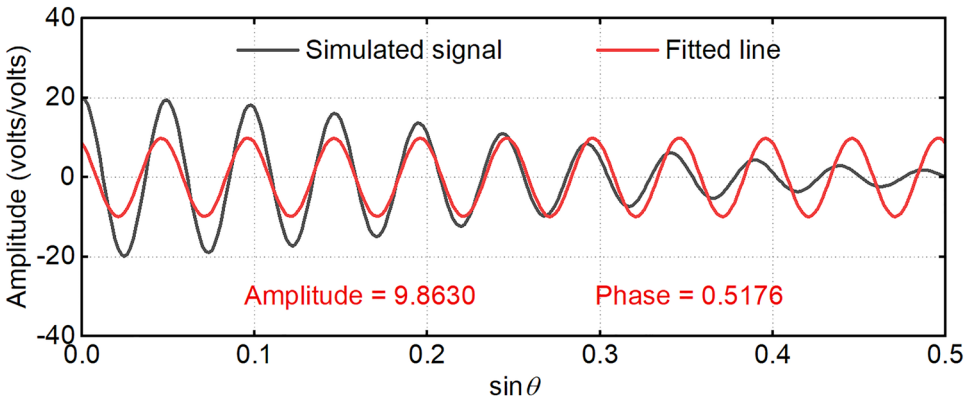


**Fig. 3** Fitting results when the fitted frequency does not match the signal frequency

elevation angles is initially acquired at a predetermined sampling interval. Subsequently, the sine values of this series are calculated. It is observed that when the fitted frequency is not equal to the signal frequency, both the amplitude and phase solutions obtained by NLS (red font in Fig. 3) deviate significantly from the true values.

To investigate the relationship between frequency difference and phase difference, the following simulation experiment was conducted. Firstly, a set of cosine signals with different frequencies were simulated, each with a fixed amplitude of 20 and an initial phase of 0. Subsequently, the frequency of the objective function was set to 20, and the NLS was utilized to solve the amplitude and phase for each simulated signal. By the fitting results, the variation in phase difference and amplitude difference with frequency difference were derived, respectively. Based on the relationship between frequency and RH, the frequency difference was further converted into the RH deviation. The resulting relationship curve is presented in Fig. 4.

As seen in Fig. 4, a one-to-one correspondence exists between the height difference (or frequency difference) and the phase difference within a certain range centered at zero. Once this range is exceeded, the phase begins to jump irregularly, at which point the change in the height difference does not cause a noticeable change in the phase difference. Whereas the variation of amplitude difference with height difference is symmetric about the zero axis, which implies that there does not exist a symmetric interval centered at zero, allowing the height difference to be uniquely determined by the amplitude difference. Therefore, we will focus on exploring the relationship between the height difference and the phase difference.

In a real observing environment, each site has a different hardware configuration, setup environment, and antenna height, leading to variations in the frequency range, data length, and noise level of SNR oscillations that they can be used to retrieve (Wang et al. 2018a). Moreover, even the SNR data from the same site may vary depending on the satellite orbit. To explore the effects of different factors on the relationship between height difference and phase difference, their relationship curves at different frequencies, elevation ranges, noise levels, and decay factors were obtained utilizing simulation data, and the results are shown in Fig. 5.

Figure 5 shows that the relationship between the height difference and the phase difference is always stable within a certain range of height difference near the zero axis, despite the changes in the frequency and noise level of the SNR oscillations. However, when the elevation range and the decay factor change, their relationship changes significantly. Among these, when the elevation range of the SNR oscillations changes, the range of height difference where this relationship stably exists also changes accordingly. In Fig. 6, the relationship curves under different frequencies and noise levels are plotted within the same coordinate system, showing only the variations within the height difference range of −0.2 to 0.2 m. As depicted, within this range, the phase difference appears to have an approximate linear relationship with the height difference. This indicates that if the

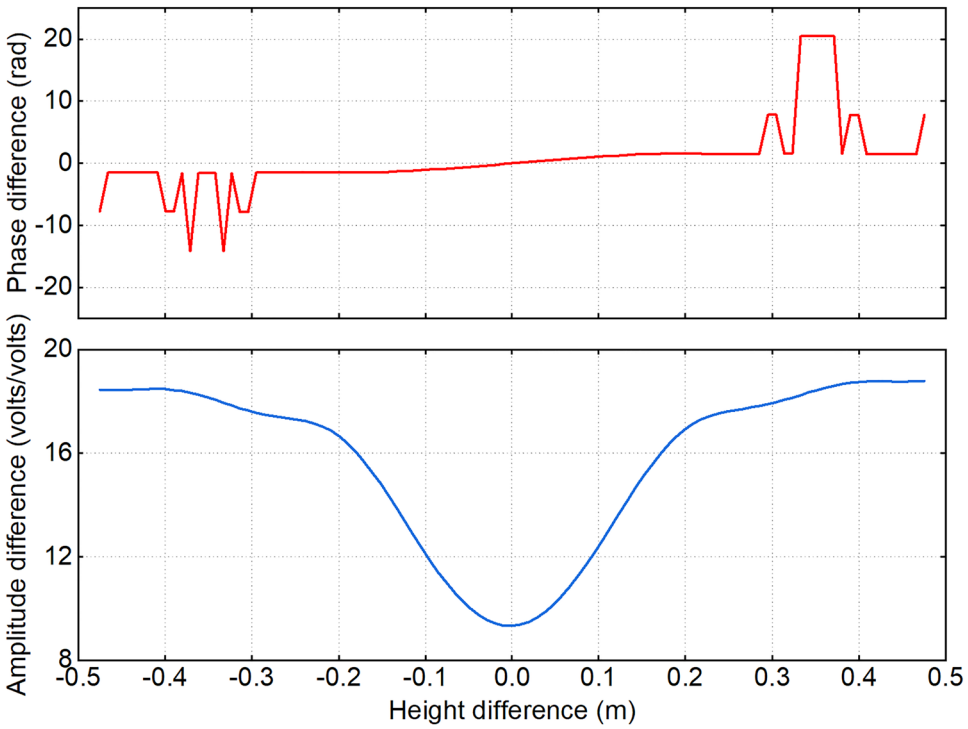


**Fig. 4** Relationship between fitting result deviations and height difference. The phase solution (top) and amplitude solution (bottom) deviations vary with the height difference, respectively

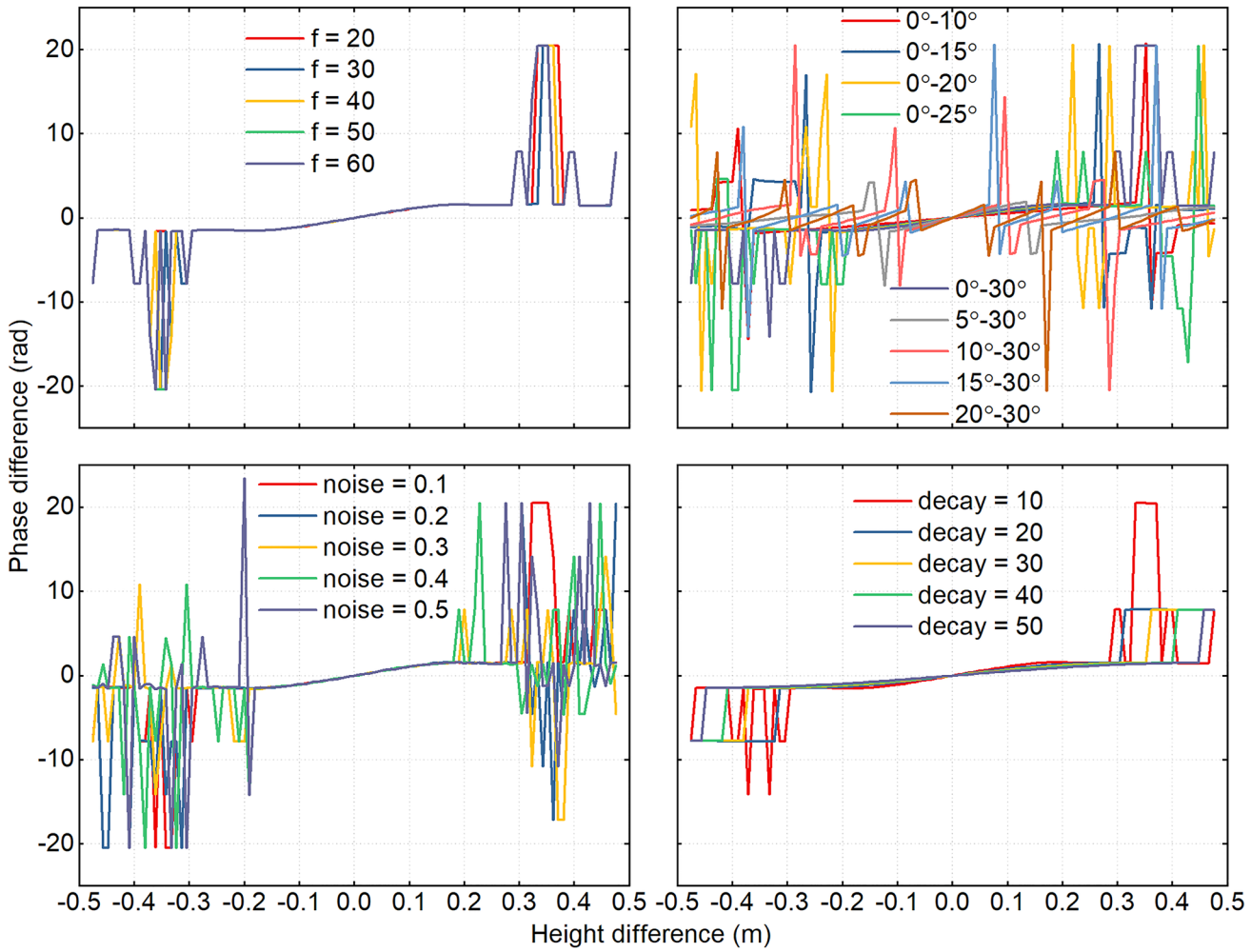


**Fig. 5** Effect of various factors on the relationship between height difference and phase difference. The relationship curves between height difference and phase difference are depicted for different frequencies (top left), elevation ranges (top right), noise levels (bottom left), and decay factors (bottom right)

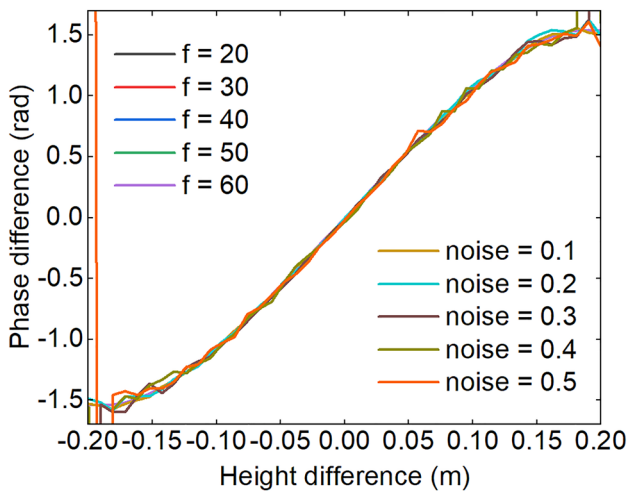


**Fig. 6** Relationship curves between height difference and phase difference at various frequencies and noise levels

differences in the elevation range and decay factor can be ignored, a stable linear relationship between the two can be established within a specific range of height difference.

During the retrieval process, using strict screening conditions, it is possible to filter and obtain the most comprehensive SNR oscillations within a given elevation range. Moreover, the decay trends of different SNR series at the same site are basically the same. In addition, for SNR oscillations from the sea surface, external environmental changes have less influence on the phase, so the relationship between height difference and phase difference can be converted into the relationship between height difference and phase. This suggests that if the relationship between the phase and the height difference is determined in the actual retrieval process, the phase can be used to correct further the retrieval error of the RH (or the sea-level estimates obtained from the frequency). Accordingly, the corrected sea-level height can be expressed as:

$$\hat{h}_{sea} = H - h + \Delta h = H - \frac{\lambda f}{2} + (a\varphi + b) \quad (10)$$

where $\Delta h$ is the retrieval error of RH, and $a$ and $b$ are the fitting coefficients. To this end, a linear phase correction GNSS-IR sea-level estimation method based on LSP-NLS is constructed in this study. Initially, this method utilizes LSP to extract the frequency of SNR oscillations. Subsequently, the acquired frequency is inputted into the NLS to solve the phase of SNR oscillations further, utilizing the phase acquired by NLS to correct the retrieval error of LSP.

## Results

Through simulation analysis, the relationship curve between height difference and phase difference has been successfully mapped. Next, the measured data will be utilized to further verify the validity and stability of the relationship in practical applications.

### Relationship between characteristic parameters of SNR oscillations and retrieval error

According to the basic principles of GNSS-IR, we processed the SNR data from the day of year (DOY) 112–123 in 2022 at the SC02 site. To ensure the data quality, SNR series within the range of 2°–12° elevation angle of the site were selected, and each SNR series within this range should contain at least 90 observations. For a valid SNR series, a cubic polynomial was first removed from the series, and then its principal frequency was extracted using LSP. To guarantee the retrieval accuracy, the frequency corresponding to the maximum peak amplitude in the periodogram was retrieved in the RH range of 4–9 m, and the retrieved values with the peak amplitude power less than 5 and the peak-to-noise ratio (the ratio of the maximum peak amplitude to the average peak amplitude of the noise in the RH range) less than 3 were removed (Song et al. 2019; Löfgren et al. 2014). The TG data were interpolated using the cubic spline method to obtain the measured sea-level heights at the moments corresponding to the estimated values, thus evaluating the accuracy of the retrieval results. To avoid the influence of outliers, the estimated values greater than the triple standard deviation in the retrieval results were removed. The retrieval results obtained from the frequency of SNR oscillations and the corresponding retrieval error are shown in Fig. 7.

From a 15-day observation, a total of 519 estimates were obtained. After calculating, the correlation coefficient ($R$) between the retrieved results and TG data is 0.9907, the root mean square error (RMSE) is 11.24 cm, and the mean absolute error (MAE) is 9.11 cm. As seen in Fig. 7, the sea-level variation obtained from the frequency agrees well with the TG data, and the retrieval error is basically within ± 20 cm. During the retrieval process, the frequency obtained from the LSP is used as the fitted frequency, while the amplitude and phase of the SNR oscillations are solved using NLS. Figure 8 (left) displays the acquired amplitude and phase over time, indicating that the directly acquired amplitude and phase series contain outliers. Using the triple standard

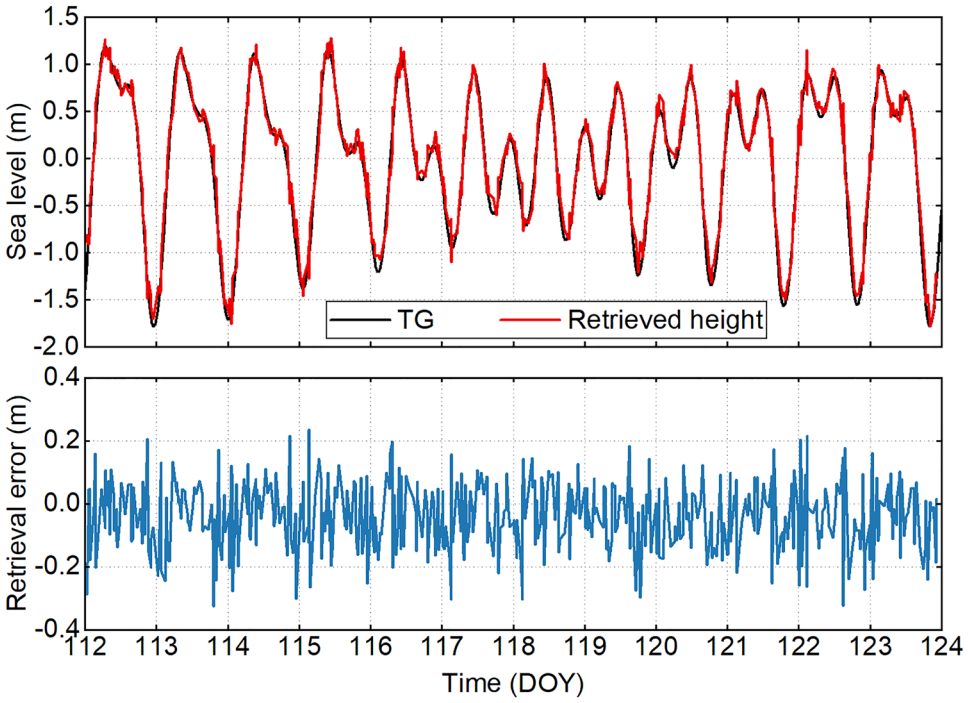


**Fig. 7** Retrieval results of DOY112-123 in 2022 at SC02 site. (Top) Retrieval results of sea-level height; (Bottom) Difference between retrieval results and TG data

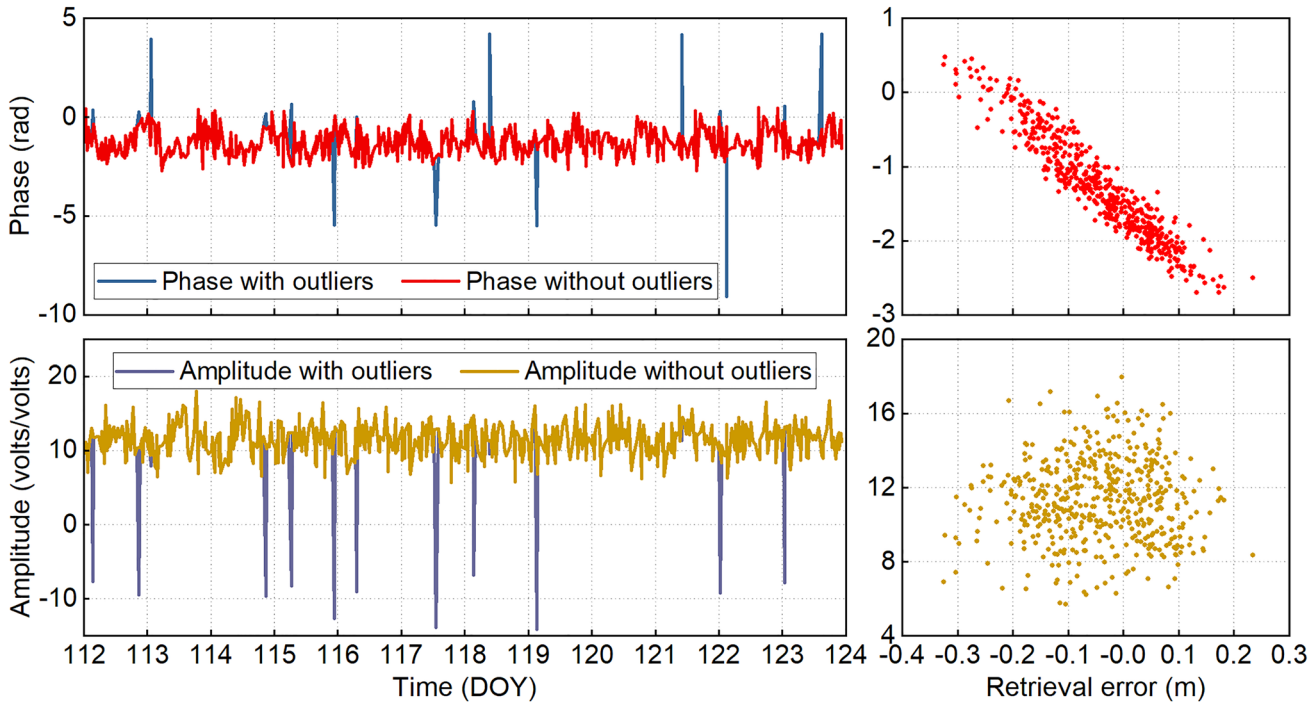


**Fig. 8** Relationship between different features and retrieval error for sea-level height. Phase (top left) and amplitude (bottom left) series before and after removing outliers, and the relationship between retrieval error and phase (top right) and amplitude (bottom right) after removing outliers, respectively

deviation method, outliers in amplitude and phase were eliminated (values at locations where outliers appeared in amplitude and phase were removed for each series). Following this, the outlier-removed amplitude and phase were compared with the frequency-based retrieval error, as shown in Fig. 8 (right).

As seen in Fig. 8 (right), there is a significant linear relationship between the phase after removing outliers and retrieval error, with the $R$ of $-0.9478$. In contrast, the amplitude does not show a clear correlation with the retrieval error, which is consistent with the results from the simulation experiment. Moreover, the amplitude of SNR oscillations is highly susceptible to the influence of the external environment, and the relationship between height difference and amplitude cannot be simply converted from that of height difference and amplitude difference. Figure 9 demonstrates the temporal variations of negative phase and retrieval error, and it can be seen that there is a strong consistency in the trend between them.

## Relationship between phase and retrieval error at different sites

To further verify the relationship between phase and retrieval error, we conducted experiments using data from four sites: SC02, GTGU, SPBY, and CALC. Among them,

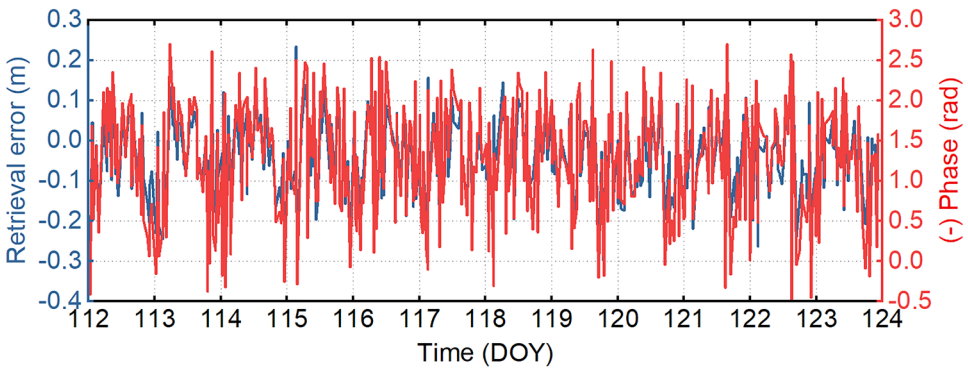


**Fig. 9** Temporal variation of retrieval error and negative phase

the GTGU site used 92 days of observational data, while the remaining three sites each used 6 months of observational data. Following the data processing procedure described in the previous section, data from the four sites were processed separately, and relevant parameters were adjusted according to the actual conditions of different sites. The accuracy statistics of retrieval results by frequency for different sites are listed in Table 2.

According to the data in Table 2, the retrieval results of all four stations have a high level of accuracy. The $R$ of their retrieval results with TG data for each site is greater than 0.9, the RMSE is less than 12 cm, and the MAE is less than 10 cm. Based on the data processing method in the previous section, the phase variations of different sites were obtained simultaneously. Figure 10 shows the error distribution of retrieval results from different sites and the correspondence between phase and retrieval error. As seen in the figure, the retrieval errors at all four sites conform to the normal distribution. The maximum error does not exceed 50 cm, and the vast majority of errors are distributed within 20 cm. Furthermore, a significant linear relationship between phase and retrieval error is consistently observed at different sites.

To accurately determine the linear relationship between retrieval error and phase for each site, we employed a two-step linear regression. Initially, a preliminary regression analysis was carried out to obtain an approximate relationship between the two. Subsequently, based on the results from the first regression, outliers deviating by more than the triple standard deviation were removed. Finally, the second regression analysis was conducted on the remaining data to derive an accurate linear model, as depicted in Fig. 10 (right). As seen in the figure, the coefficients of determination ($R^2$) for the linear regression model at each site are above 0.8. This suggests that the derived linear equations can satisfactorily explain the relationship between retrieval error and phase. As seen from the relationship equations derived at different sites, those obtained for SC02, GTGU, and SPBY are relatively close to each other, while those for CALC differ significantly from those of the other three sites. Additionally, the distribution range of phases at CALC is significantly larger than that at the other three sites. Notably, the interval range of SNR data used for retrieval at CALC is distinctly different from that of the other three sites. From the results of simulation experiments, the difference in sample intervals has a significant effect on the relationship between the two. In addition, the sites differed in their placement environments and the parameters used in the retrieval process. These factors collectively contribute to discrepancies in the relationship models obtained from different sites. Consequently, we cannot find a uniform relationship equation to accurately describe the relationship between phase and retrieval error for all sites. However, considering the $R^2$ of regression results for each site, we can confirm that there is a long-term stable relationship between phase and retrieval error within at least one site.

**Table 2** Accuracy statistics of retrieval results from different sites

| Sites and periods | $R$ | RMSE (cm) | MAE (cm) | Number of values |
|---|---|---|---|---|
| SC02<br>DOY 1–181 in 2022 | 0.9917 | 11.79 | 9.21 | 7894 |
| GTGU<br>DOY 274–365 in 2015 | 0.9520 | 8.95 | 6.72 | 4661 |
| SPBY<br>DOY 1–181 in 2019 | 0.9294 | 10.36 | 8.24 | 3683 |
| CALC<br>DOY 1–182 in 2020 | 0.9369 | 9.05 | 7.17 | 5605 |

## Retrieval result based on phase correction

In the preceding section, the relationship models between phase and frequency-based retrieval error for different sites were obtained from nearly 6 months of retrieval results. This means that by simply substituting them into (10), the phase can be utilized to correct the retrieval error, thus further improving the accuracy of retrieval results. To verify the effectiveness of this method, we processed the SNR data for the next 6 months at the four sites, using both the traditional method (frequency) and the linear phase correction method based on LSP-NLS (frequency + phase) to retrieve the sea-level height. The precision indexes of retrieval results obtained by the two methods are given in Table 3, and the differences between the retrieval results of the two methods and TG data are compared in Fig. 11 (to show the differences more clearly, only 1-month sea-level variations are shown here).

As shown in Table 3, the $R$ of retrieval results after phase correction for different sites and TG data all reach 0.99, the RMSE is around 4.0 cm, and the MAE is less than 3.5 cm. Compared to the traditional method using only frequency, the retrieval accuracy after phase correction is greatly improved. Among them, the RMSE and MAE of SC02 are reduced by 66.53% and 66.63%, respectively, with the largest improvement effect, while the RMSE and MAE of CALC are reduced by 55.98% and 54.94%, respectively, with the smallest improvement effect. Additionally, it is noteworthy that the quantity of retrieval results derived from the phase correction method is slightly fewer than the traditional method. This discrepancy arises because the phase correction method eliminates outliers within the phase series during retrieval. From Fig. 11, it is clear that the retrieval results after phase correction are more consistent with the actual sea-level variations than the traditional method using only frequency. To further illustrate the effect of phase correction, Fig. 12 depicts the error distribution of retrieval results

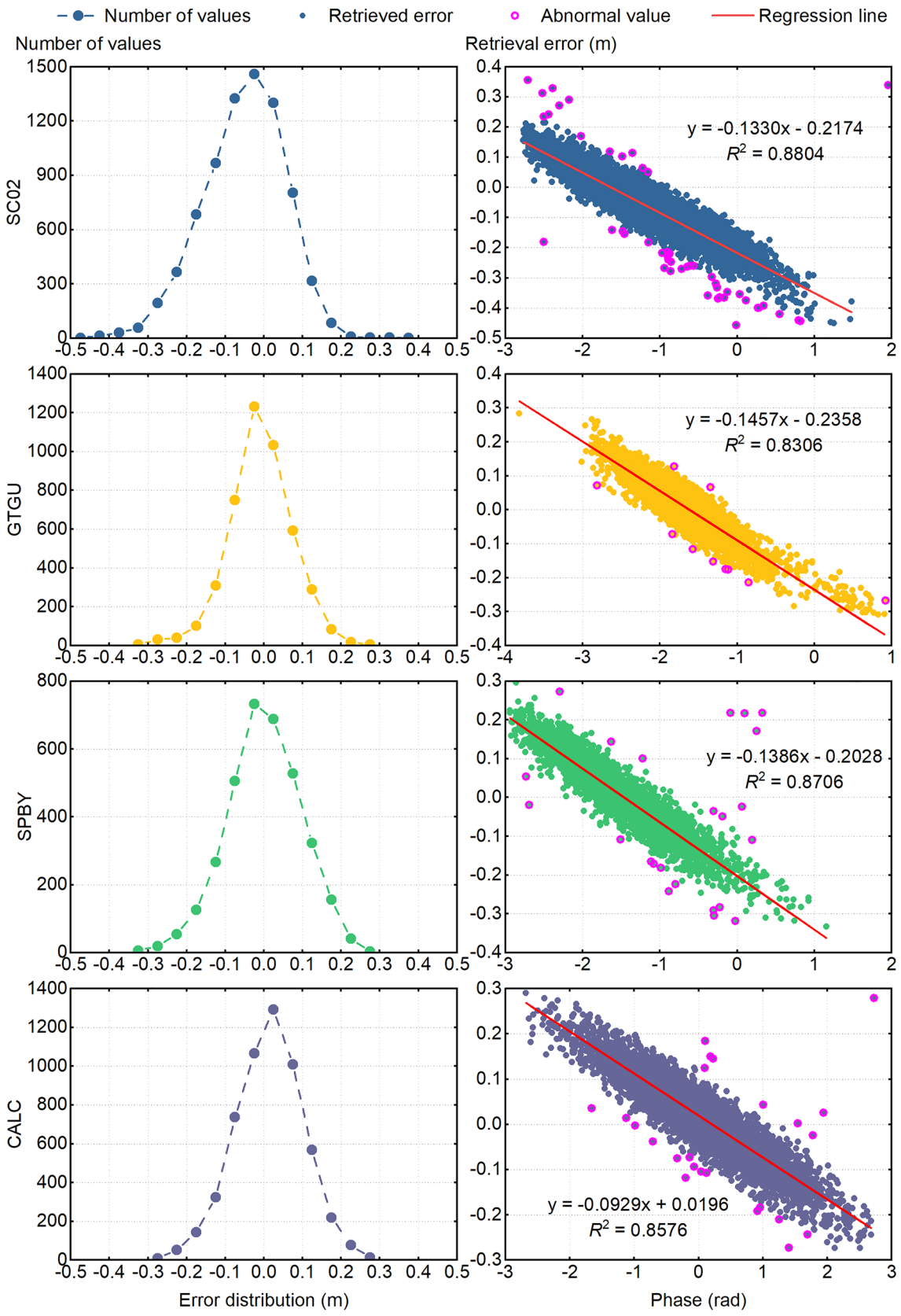


**Fig. 10** For different sites (each row), the distribution of retrieval error (left) and their relationship with phase difference (right)

**Table 3** Precision statistics of retrieval results from different methods at each site

| Sites and periods | Method | *R* | RMSE (cm) | MAE (cm) | Number of values |
|---|---|---|---|---|---|
| SC02 DOY 182–365 in 2022 | Frequency | 0.9921 | 11.56 | 9.08 | 8151 |
| | Frequency + phase | 0.9993 | 3.87 | 3.03 | 7953 |
| GTGU DOY 1–80 in 2016 | Frequency | 0.9400 | 9.22 | 7.08 | 4089 |
| | Frequency + phase | 0.9925 | 3.53 | 2.77 | 3932 |
| SPBY DOY 182–365 in 2019 | Frequency | 0.9351 | 10.16 | 7.95 | 3776 |
| | Frequency + phase | 0.9927 | 4.08 | 3.18 | 3476 |
| CALC DOY 183–366 in 2020 | Frequency | 0.9552 | 8.96 | 7.11 | 5544 |
| | Frequency + phase | 0.9913 | 3.94 | 3.20 | 5494 |

obtained by different methods from the four stations. As evidenced in the figure, the phase can effectively correct retrieval errors, thereby enhancing the precision of retrieval results.

## Discussion

The results of simulation experiments show that the elevation range of SNR oscillations and their decay level are the critical factors affecting the relationship between the two. Among them, the decay level of SNR oscillations is affected by the physical characteristics of reflecting surface and environment factors, while the elevation range is related to our screening strategy and interval selection (Ran et al. 2022; Wang et al. 2022). The analysis results of measured data also confirm that the choice of elevation range can cause significant variations in the relationship model between different sites. Therefore, we simulated the solving process of NLS to explore the correlation between its solution and the sample intervals.

According to the basic principles of GNSS-IR, the SNR oscillations can be approximated as a cosine function, and the frequency of the objective function is already determined before using the NLS. Hence, the solution process can be transformed into an alignment process between two signals. Given a cosine wave $y_1 = A_1 \cos\left(2\pi f_1 t + \varphi_1\right)$ and another cosine wave $y_2 = A\cos\left(2\pi f_2 t + \varphi\right)$ with a close but different frequency, this cosine wave can be stretched vertically and shifted horizontally by adjusting the amplitude $A$ and phase $\varphi$. According to the equation of the two cosine signals, the difference between them at a certain moment can be obtained as:

$$\Delta y = y_1 - y_2 = A_1 \cos\left(2\pi f_1 t + \varphi_1\right) - A\cos\left(2\pi f_2 t + \varphi\right) \tag{11}$$

For any set of $A$ and $\varphi$, the sum of squared residuals between the two signals within the time range $[t_1, t_2]$ can be expressed as:

$$SSR_{(A,\varphi)} = \int_{t_1}^{t_2} \left[A_1 \cos\left(2\pi f_1 t + \varphi_1\right) - A\cos\left(2\pi f_2 t + \varphi\right)\right]^2 dt \tag{12}$$

When the *SSR* reaches its minimum value, the two signals align, at this point, the amplitude and phase are likewise the solution of NLS. According to (12) and combined with the basic properties of trigonometric functions, it can be derived:

$$\begin{aligned} SSR_{(-A,\varphi+(2n-1)\pi)} &= SSR_{(A,\varphi)} \\ SSR_{(A,\varphi+2n\pi)} &= SSR_{(A,\varphi)} \end{aligned} \tag{13}$$

where $n$ is an integer. From (13), the *SSR* in the $\varphi$-direction is of periodic character with a period of $2\pi$. Under the action of negative amplitude, there is another equivalent solution within a period, and the difference between the two solutions is $\pi$. Although it is impossible to derive its analytical solutions from (12) directly, we can explore their variation patterns through simulation data. Setting the amplitude, frequency, and phase of the fixed signal to 20, 40, and 0, respectively, and the frequency of the dynamic signal to 39, the variation of *SSR* in the amplitude and phase directions is shown in Fig. 13.

As seen in Fig. 13 (right), when there is a difference in frequency between the two signals, the phase solution no longer converges to the zero-axis position. The minima closest to the actual phase are distributed on either side of the zero axis, with these two positions having a phase difference of $\pi$ and opposite amplitudes. These are our two most accessible solutions because the initialization parameters are typically set in the vicinity of the true values when using NLS (as shown in Fig. 8 for the outliers of the amplitude). Manifestly, when a negative amplitude solution is obtained, phase correction is required to ensure the effective range of the phase remains unchanged. While we often attribute the occurrence of outlier solutions to local optima, the periodic variation of *SSR* indicates that there is no so-called "global optimum".

Figure 14 shows the relative position between the two signals and their difference for different values of $\varphi$ when

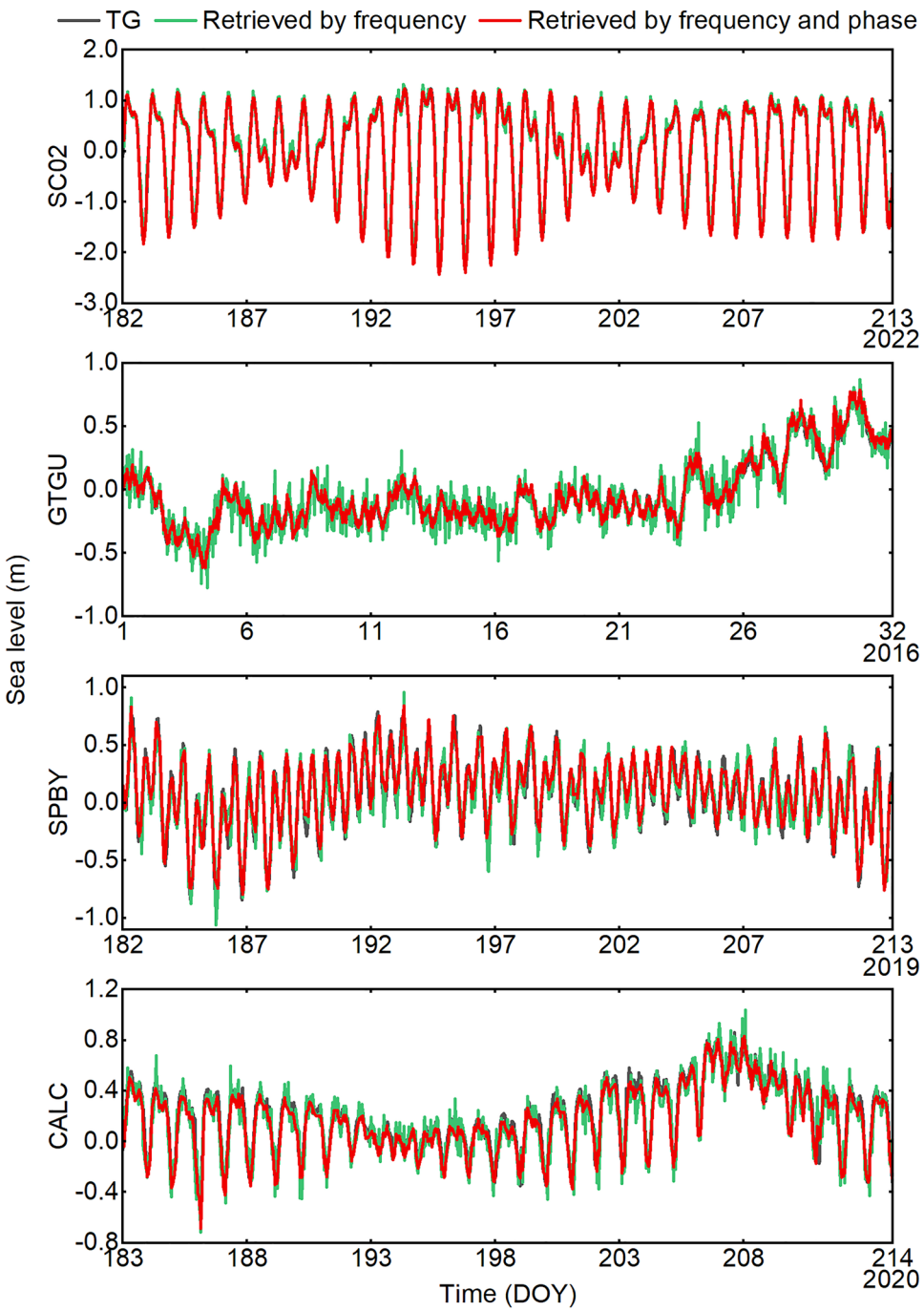


**Fig. 11** Differences between the retrieval results from different methods and TG data at each site

the amplitude is fixed at 20. As can be seen, a short-distance region exists between two cosine signals of different frequencies. Due to the periodicity of the cosine signal, changes in amplitude clearly cannot alter the relative position of this region on the coordinate axis. As $\varphi$ changes, the relative positions between the two signals shift, moving the location of this region along the axis. This shows that if the effect of the data sampling interval is ignored, by adjusting the phase, it is possible to move the minimum difference formed in a specific interval to any equivalent-length interval. Hence, when using NLS to solve the phase of a cosine signal, if there is a difference between the fitted frequency and the actual frequency of the signal, the phase solution obtained is only the optimal solution for the given sample interval. Changes in the sample interval will alter the phase solution, at which point the phase loses its inherent physical meaning (as depicted in Fig. 15). Even considering the decay features of the signal, this pattern still holds, but the amplitude also changes with the sample interval.

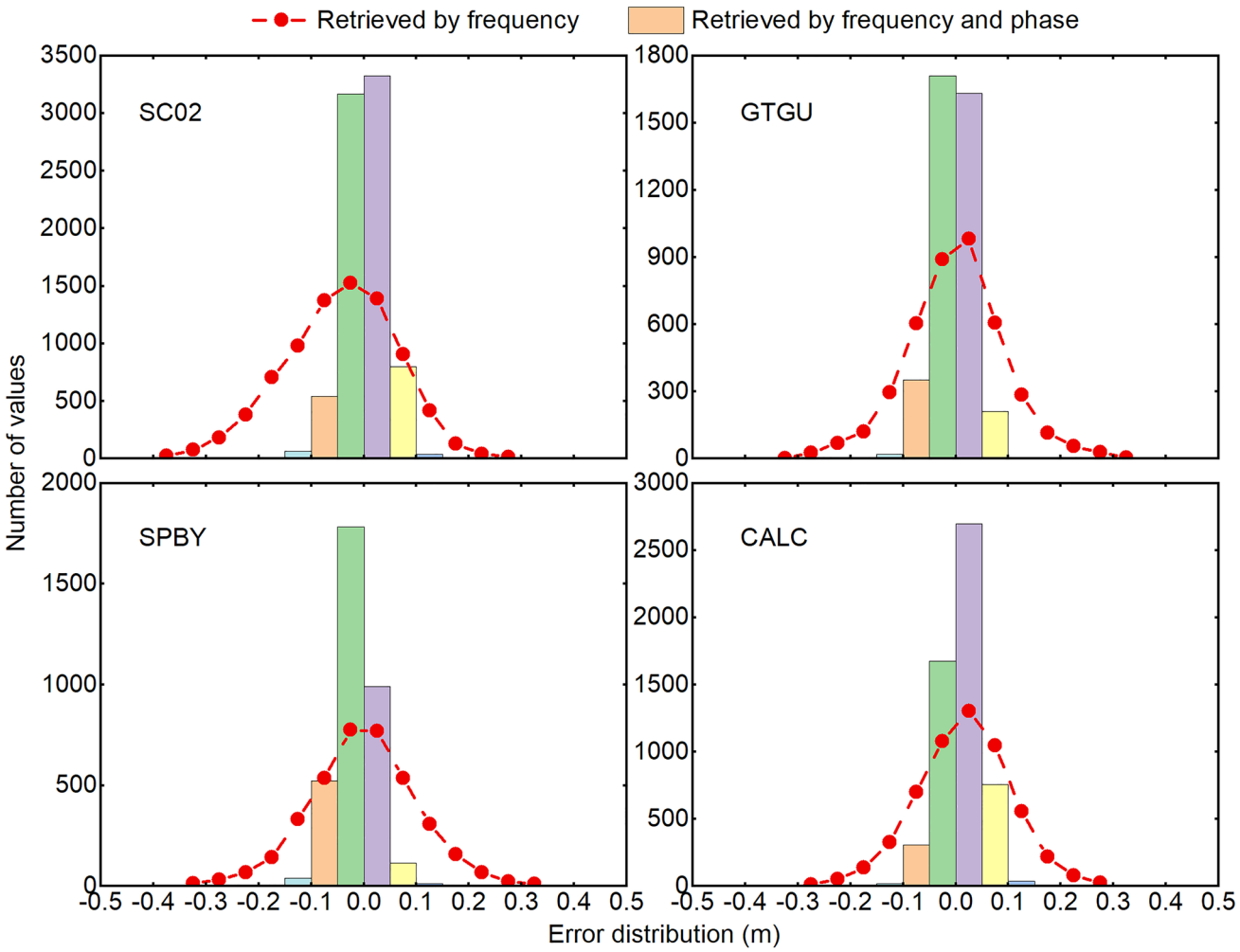


**Fig. 12** Error distribution of retrieval results at each site

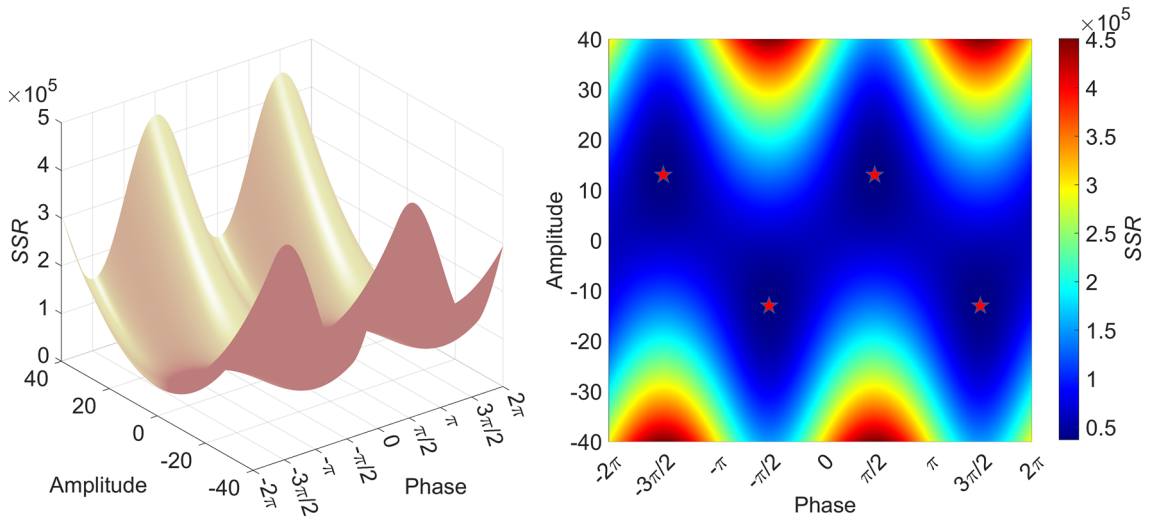


**Fig. 13** Variation of *SSR* between the two signals in terms of amplitude and phase. (Left) three-dimensional; (Right) two-dimensional, where the red pentagram indicates the minimum points of *SSR* in both variable directions

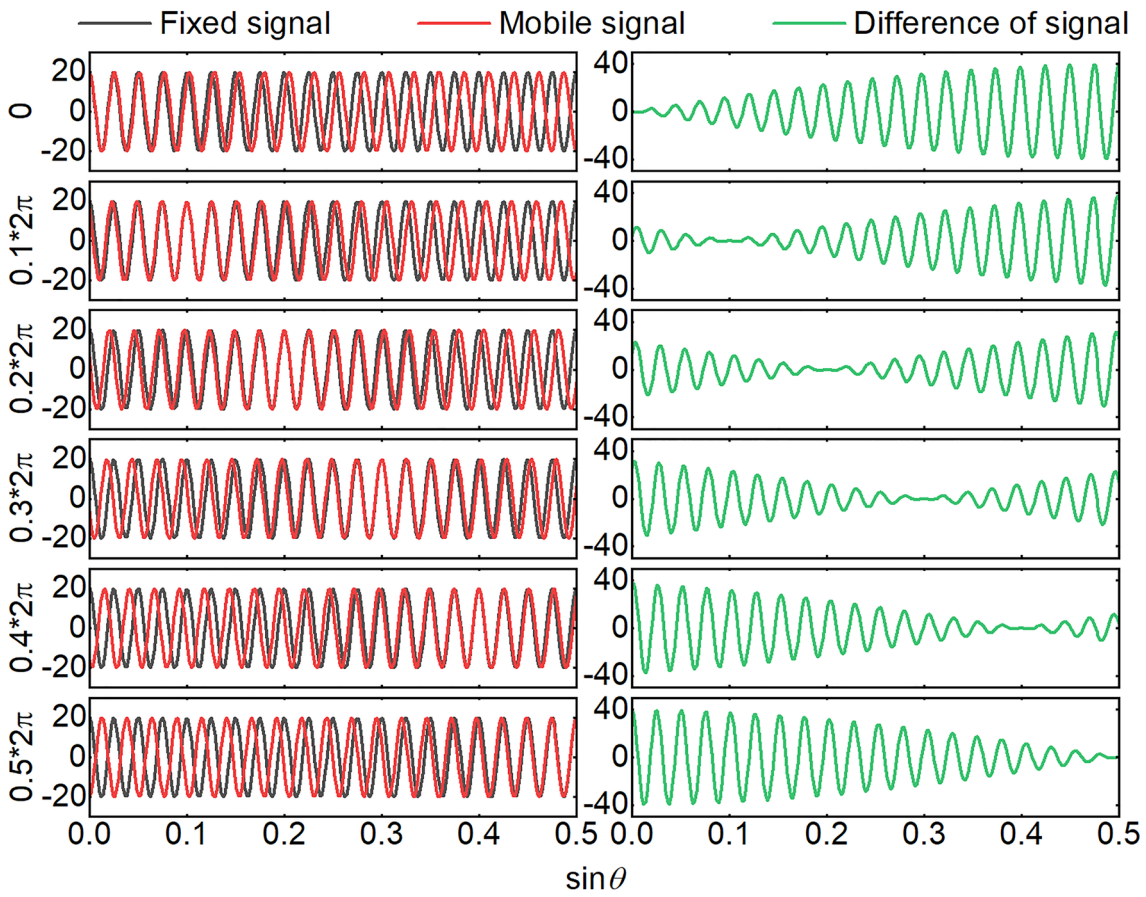


**Fig. 14** For different values of $\varphi$ (each row), the relative position between two signals (left) and the difference between their corresponding points (right)

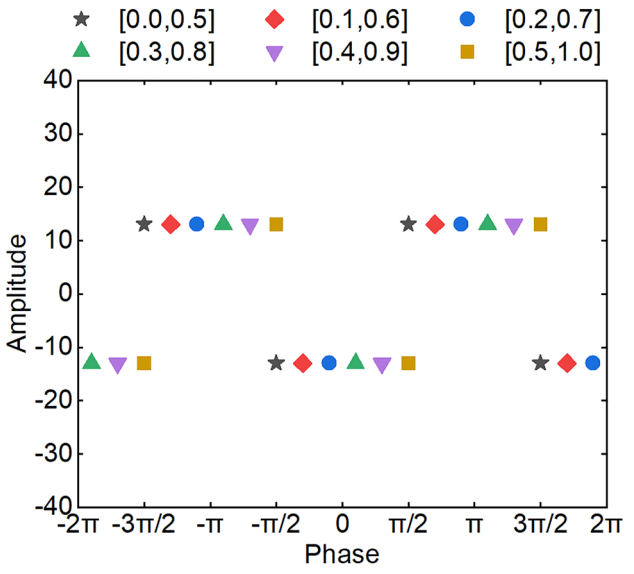


**Fig. 15** Variation of the minimum points of *SSR* with sample intervals. To ensure consistency across intervals, equal interval sampling is used here

## Conclusions

In the GNSS-IR technique, LSP and NLS are the crucial methods to obtain the characteristic parameters of SNR oscillation. Limited by the quality of SNR data itself and the retrieval accuracy of LSP, there is always a certain difference between the acquired and actual frequencies of SNR oscillations. However, when using NLS to fit cosine signals, the precision of amplitude and phase solutions depends greatly on the accuracy of fitted frequencies.

Through simulation analysis, we identified that when there is some difference between the fitted frequency and the actual signal frequency, the phase difference shows a clear linear relationship with the frequency difference. Moreover, the stability of this relationship in continuous monitoring was verified through the retrieval results of nearly half a year from the SC02, GTGU, SPBY, and CALC sites. However, the data ranges and parameter settings used vary from site to site, resulting in different regression models obtained from different sites.

Based on this, a linear phase correction GNSS-IR sea-level estimation method based on LSP-NLS is developed

in this study. The method combines LSP and NLS to process SNR oscillations, and the phase acquired by NLS is utilized to correct the retrieval error of LSP. Using this method, the regression models obtained from the four stations were utilized to retrieve the sea-level variation at each station for the next 6 months. The results show that the frequency difference information embedded in the phase can effectively correct the retrieval error of LSP, thus improving the retrieval accuracy. Compared with the traditional method using only frequency, the RMSE and MAE of retrieval results obtained by the linear phase correction method based on LSP-NLS are reduced by about 60%.

Although NLS is a critical method in the GNSS-IR technique, it is the first time that the method is used to process SNR oscillations during sea-level estimation in this study, as well as the first time that phase is used to estimate sea-level height. Additionally, while we mainly focused on sea-level estimation in this study, the relationship between frequency difference and phase also holds valuable application and guidance in other GNSS-IR domains. Currently, further consolidation of these findings is underway.

**Acknowledgements** The authors are very grateful to all the organizations and institutions that provided data support for this study.

**Authors contributions** Zhenkui Wei: methodology, software, writing—original draft. Chao Ren: conceptualization, funding acquisition, writing—review and editing. Yueji Liang: conceptualization, funding acquisition, writing—review and editing. Yintao Liu: formal analysis, validation, visualization. Jieyu Liang: project administration, software. Anchao Yin: supervision, validation. Weiting Yue: software, validation. Xudong Zhang: supervision, validation. Xiaoqi Lin: software, validation.

**Funding** This work was supported by the National Natural Science Foundation of China (Grant Nos. 42064003, 41901409) and the Guangxi Natural Science Foundation (Grant No. 2021GXNSFBA220046).

**Availability of data and materials** The GNSS data for the SC02, SPBY, and CALC sites are provided by UNAVCO (https://www.unavco.org/), GA (https://www.ga.gov.au/), and the National Geodetic Survey (https://www.ngs.noaa.gov/), respectively. The tidal gauge data at Friday Harbor and Calcasieu Pass are supplied by NOAA (https://tidesandcurrents.noaa.gov/), while data at Spring Bay is furnished by the Intergovernmental Oceanographic Commission (http://www.ioc-sealevelmonitoring.org/). Additionally, the GNSS and tide gauge data for the GTGU site are derived from the dataset shared in the Zenodo from the first IAG inter-comparison campaign (https://www.zenodo.org/record/2924309).

## Declarations

**Competing interests** The authors declare that they have no known competing financial interests or personal relationships that could have appeared to influence the work reported in this paper.



## References

Bilich A, Larson KM (2007) Correction published 29 March 2008: mapping the GPS multipath environment using the signal-to-noise ratio (SNR). Radio Sci 42(06):1–16. https://doi.org/10.1029/2007RS003652

Chew CC, Small EE, Larson KM, Zavorotny VU (2013) Effects of near-surface soil moisture on GPS SNR data: development of a retrieval algorithm for soil moisture. IEEE Trans Geosci Remote Sens 52(1):537–543. https://doi.org/10.1109/TGRS.2013.2242332

Chew C, Small EE, Larson KM (2016) An algorithm for soil moisture estimation using GPS-interferometric reflectometry for bare and vegetated soil. GPS Solut 20:525–537. https://doi.org/10.1007/s10291-015-0462-4

Geremia-Nievinski F, Hobiger T, Haas R, Liu W, Strandberg J, Tabibi S, Vey S, Wickert J, Williams S (2020) SNR-based GNSS reflectometry for coastal sea-level altimetry: results from the first IAG inter-comparison campaign. J Geodesy 94(8):70. https://doi.org/10.1007/s00190-020-01387-3

Hu Y, Yuan X, Liu W, Wickert J, Jiang Z, Haas R (2021) GNSS-IR model of sea level height estimation combining variational mode decomposition. IEEE J Sel Top Appl Earth Obs Remote Sens 14:10405–10414. https://doi.org/10.1109/JSTARS.2021.3118398

Ilyushin YA, Padokhin AM, Smolov VE (2019) Global navigational satellite system phase altimetry of the sea level: Systematic bias effect caused by sea surface waves. In: 2019 photonics and electromagnetics research symposium-spring (PIERS-Spring). IEEE 2019, pp 1618–1627.https://doi.org/10.1109/PIERS-Spring46901.2019.9017826

Larson KM, Nievinski FG (2013) GPS snow sensing: results from the EarthScope Plate Boundary Observatory. GPS Solut 17:41–52. https://doi.org/10.1007/s10291-012-0259-7

Larson KM, Small EE, Gutmann ED, Bilich AL, Braun JJ, Zavorotny VU (2008) Use of GPS receivers as a soil moisture network for water cycle studies. Geophys Res Lett. https://doi.org/10.1029/2008GL036013

Larson KM, Gutmann ED, Zavorotny VU, Braun JJ, Williams MW, Nievinski FG (2009) Can we measure snow depth with GPS receivers? Geophys Res Lett. https://doi.org/10.1029/2009GL039430

Larson KM, Löfgren JS, Haas R (2013a) Coastal sea level measurements using a single geodetic GPS receiver. Adv Space Res 51(8):1301–1310. https://doi.org/10.1016/j.asr.2012.04.017

Larson KM, Ray RD, Nievinski FG, Freymueller JT (2013b) The accidental tide gauge: a GPS reflection case study from Kachemak Bay, Alaska. IEEE Geosci Remote Sens Lett 10(5):1200–1204. https://doi.org/10.1109/LGRS.2012.2236075

Larson KM, Ray RD, Williams SD (2017) A 10-year comparison of water levels measured with a geodetic GPS receiver versus a conventional tide gauge. J Atmos Ocean Technol 34(2):295–307. https://doi.org/10.1175/JTECH-D-16-0101.1

Larson KM, Lay T, Yamazaki Y, Cheung KF, Ye L, Williams SD, Davis JL (2021) Dynamic sea level variation from GNSS: 2020 Shumagin earthquake tsunami resonance and Hurricane Laura. Geophys Res Lett 48(4):e2020GL091378. https://doi.org/10.1029/2020GL091378

Li J, Hong X, Wang F, Yang L, Yang D (2023) Simultaneous retrieval of corn growth status and soil water content based on one GNSS antenna. Remote Sens 15(7):1738. https://doi.org/10.3390/rs15071738

Löfgren JS, Haas R, Scherneck HG (2014) Sea level time series and ocean tide analysis from multipath signals at five GPS sites in different parts of the world. J Geodyn 80:66–80. https://doi.org/10.1016/j.jog.2014.02.012

Lomb NR (1976) Least-squares frequency analysis of unequally spaced data. Astrophys Space Sci 39:447–462. https://doi.org/10.1007/BF00648343

Marquardt DW (1963) An algorithm for least-squares estimation of nonlinear parameters. J Soc Ind Appl Math 11(2):431–441. https://doi.org/10.1137/0111030

Martín A, Luján R, Anquela AB (2020) Python software tools for GNSS interferometric reflectometry (GNSS-IR). GPS Solut 24(4):94. https://doi.org/10.1007/s10291-020-01010-0

Nievinski FG, Larson KM (2014) Forward modeling of GPS multipath for near-surface reflectometry and positioning applications. GPS Solut 18:309–322. https://doi.org/10.1007/s10291-013-0331-y

Peng D, Hill EM, Li L, Switzer AD, Larson KM (2019) Application of GNSS interferometric reflectometry for detecting storm surges. GPS Solut 23:1–11. https://doi.org/10.1007/s10291-019-0838-y

Purnell D, Gomez N, Chan NH, Strandberg J, Holland DM, Hobiger T (2020) Quantifying the uncertainty in ground-based GNSS-reflectometry sea level measurements. IEEE J Sel Top Appl Earth Observ Remote Sens 13:4419–4428. https://doi.org/10.1109/JSTARS.2020.3010413

Ran Q, Zhang B, Yao Y, Yan X, Li J (2022) Editing arcs to improve the capacity of GNSS-IR for soil moisture retrieval in undulating terrains. GPS Solut 26:1–11. https://doi.org/10.1007/s10291-021-01206-y

Roussel N, Ramillien G, Frappart F, Darrozes J, Gay A, Biancale R, Striebig N, Hanquiez V, Bertin X, Allain D (2015) Sea level monitoring and sea state estimate using a single geodetic receiver. Remote Sens Environ 171:261–277. https://doi.org/10.1016/j.rse.2015.10.011

Santamaría-Gómez A, Watson C (2017) Remote leveling of tide gauges using GNSS reflectometry: case study at Spring Bay, Australia. GPS Solut 21:451–459. https://doi.org/10.1007/s10291-016-0537-x

Scargle JD (1982) Studies in astronomical time series analysis. II-Statistical aspects of spectral analysis of unevenly spaced data. Astrophys J 263:835–853. https://doi.org/10.1086/160554

Song M, He X, Wang X, Zhou Y, Xu X (2019) Study on the quality control for periodogram in the determination of water level using the GNSS-IR technique. Sensors 19(20):4524. https://doi.org/10.3390/s19204524

Strandberg J, Hobiger T, Haas R (2016) Improving GNSS-R sea level determination through inverse modeling of SNR data. Radio Sci 51(8):1286–1296. https://doi.org/10.1002/2016RS006057

Strandberg J, Hobiger T, Haas R (2019) Real-time sea-level monitoring using Kalman filtering of GNSS-R data. GPS Solut 23(3):61. https://doi.org/10.1007/s10291-019-0851-1

VanderPlas JT (2018) Understanding the lomb–scargle periodogram. Astrophys J Suppl Ser 236(1):16. https://doi.org/10.3847/1538-4365/aab766

Vey S, Güntner A, Wickert J, Blume T, Ramatschi M (2016) Long-term soil moisture dynamics derived from GNSS interferometric reflectometry: a case study for Sutherland, South Africa. GPS Solut 20:641–654. https://doi.org/10.1007/s10291-015-0474-0

Wang X, Zhang Q, Zhang S (2018a) Azimuth selection for sea level measurements using geodetic GPS receivers. Adv Space Res 61(6):1546–1557. https://doi.org/10.1016/j.asr.2018.01.002

Wang X, Zhang Q, Zhang S (2018b) Water levels measured with SNR using wavelet decomposition and Lomb–Scargle periodogram. GPS Solut 22:1–10. https://doi.org/10.1007/s10291-017-0684-8

Wang X, He X, Zhang Q (2019a) Evaluation and combination of quad-constellation multi-GNSS multipath reflectometry applied to sea level retrieval. Remote Sens Environ 231:111229. https://doi.org/10.1016/j.rse.2019.111229

Wang X, Zhang Q, Zhang S (2019b) Sea level estimation from SNR data of geodetic receivers using wavelet analysis. GPS Solut 23:1–14. https://doi.org/10.1007/s10291-018-0798-7

Wang X, He X, Shi J, Chen S, Niu Z (2022) Estimating sea level, wind direction, significant wave height, and wave peak period using a geodetic GNSS receiver. Remote Sens Environ 279:113135. https://doi.org/10.1016/j.rse.2022.113135

Williams SDP, Nievinski FG (2017) Tropospheric delays in ground-based GNSS multipath reflectometry—experimental evidence from coastal sites. J Geophys Res Solid Earth 122(3):2310–2327. https://doi.org/10.1002/2016JB013612

Zhang S, Wang T, Wang L, Zhang J, Peng J, Liu Q (2021) Evaluation of GNSS-IR for retrieving soil moisture and vegetation growth characteristics in wheat farmland. J Surv Eng 147(3):04021009. https://doi.org/10.1061/(ASCE)SU.1943-5428.0000355



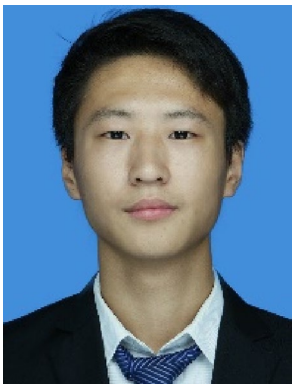

**Zhenkui Wei** is currently a graduate student in the College of Geomatics and Geoinformation of Guilin University of Technology. His current research focuses on GNSS-IR data processing and sea level estimation.

**Chao Ren** is a professor at the college of Geomatics and Geoinformation at Guilin University of Technology. He received his Ph.D. degree at Institute of Geodesy and Geophysics at Chinese Academy of Sciences in 2005. He is mainly engaged in the research of GNSS data processing and application, remote sensing technology application.

**Yueji Liang** is currently a lecturer in the college of Geomatics and Geoinformation at Guilin University of Technology. His current research focuses on the joint interpretation of surface environmental parameters by star-ground GNSS remote sensing.

**Yintao Liu** is currently a lecturer in the college of Geomatics and Geoinformation at Guilin University of Technology. His research interests focus on GNSS data processing and high-precision positioning.

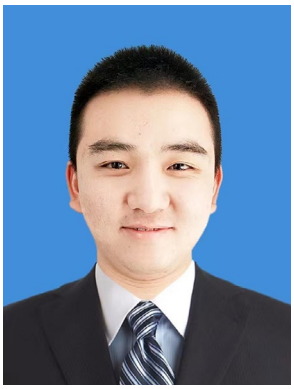

**Jieyu Liang** is currently a graduate student in the College of Geomatics and Geoinformation of Guilin University of Technology. His research interests focus on crop identification based on multi-source remote sensing images.

**Anchao Yin** is currently a graduate student in the College of Geomatics and Geoinformation of Guilin University of Technology. His current research focuses on semantic segmentation and intelligent interpretation of remote sensing images.

**Weiting Yue** is currently a graduate student in the College of Geomatics and Geoinformation of Guilin University of Technology. His research interests focus on natural disaster monitoring and prediction.

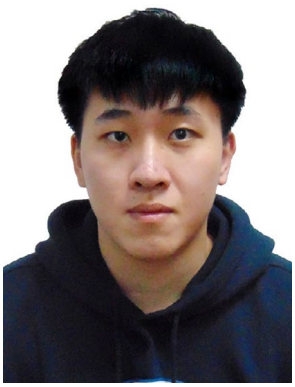

**Xudong Zhang** is currently a graduate student in the College of Geomatics and Geoinformation of Guilin University of Technology. His current research focuses on GNSS-IR data processing and soil moisture retrieval.

**Xiaoqi Lin** is currently a graduate student in the College of Geomatics and Geoinformation of Guilin University of Technology. His research interests focus on remote sensing data processing and application.